The Astrophysical Journal Letters, 954:L28 (12pp), 2023 September 1 https://doi.org/10.3847/2041-8213/acf0ba

AT 2022aedm and a New Class of Luminous, Fast-cooling Transients in Elliptical Galaxies

M. Nicholl[1], S. Srivastav[1], M. D. Fulton[1], S. Gomez[2], M. E. Huber[3], S. R. Oates[4,5], P. Ramsden[4,5], L. Rhodes[6], S. J. Smartt[1,6], K. W. Smith[1], A. Aamer[1,4,5], J. P. Anderson[7,8], F. E. Bauer[8,9,10], E. Berger[11], T. de Boer[3], K. C. Chambers[3], P. Charalampopoulos[12], T.-W. Chen[13], R. P. Fender[6], M. Fraser[14], H. Gao[3], D. A. Green[15], L. Galbany[16,17], B. P. Gompertz[4,5], M. Gromadzki[18], C. P. Gutiérrez[16,17], D. A. Howell[19,20], C. Inserra[21], P. G. Jonker[22,23], M. Kopsacheili[16,17], T. B. Lowe[3], E. A. Magnier[3], C. McCully[19], S. L. McGee[4,5], T. Moore[1], T. E. Müller-Bravo[16,17], M. Newsome[19,20], E. Padilla Gonzalez[19,20], C. Pellegrino[19,20], T. Pessi[24], M. Pursiainen[25], A. Rest[26,27], E. J. Ridley[4,5], B. J. Shappee[3], X. Sheng[1], G. P. Smith[4], G. Terreran[19,20], M. A. Tucker[28,29,30,36], J. Vinkó[31,32,33,34], R. J. Wainscoat[3], P. Wiseman[35], and D. R. Young[1]

[1] Astrophysics Research Centre, School of Mathematics and Physics, Queens University Belfast, Belfast BT7 1NN, UK; matt.nicholl@qub.ac.uk
[2] Space Telescope Science Institute (STScI), 3700 San Martin Drive, Baltimore, MD 21218, USA
[3] Institute for Astronomy, University of Hawaii, 2680 Woodlawn Drive, Honolulu, HI 96822, USA
[4] School of Physics and Astronomy, University of Birmingham, Birmingham B15 2TT, UK
[5] Institute for Gravitational Wave Astronomy, University of Birmingham, Birmingham B15 2TT, UK
[6] Department of Physics, University of Oxford, Denys Wilkinson Building, Keble Road, Oxford OX1 3RH, UK
[7] European Southern Observatory, Alonso de Córdova 3107, Casilla 19, Santiago, Chile
[8] Millennium Institute of Astrophysics MAS, Nuncio Monsenor Sotero Sanz 100, Off. 104, Providencia, Santiago, Chile
[9] Instituto de Astrofísica, Facultad de Física, Pontificia Universidad Católica de Chile, Campus San Joaquín, Av. Vicuña Mackenna 4860, Macul Santiago, 7820436, Chile
[10] Centro de Astroingeniería, Facultad de Física, Pontificia Universidad Católica de Chile, Campus San Joaquín, Av. Vicuña Mackenna 4860, Macul Santiago, 7820436, Chile
[11] Center for Astrophysics | Harvard & Smithsonian, Cambridge, MA 02138, USA
[12] Department of Physics and Astronomy, University of Turku, Vesilinnantie 5, FI-20500, Finland
[13] Technische Universität München, TUM School of Natural Sciences, Physik-Department, James-Franck-Straße 1, D-85748 Garching, Germany
[14] School of Physics, O'Brien Centre for Science North, University College Dublin, Belfield, Dublin 4, Ireland
[15] Astrophysics Group, Cavendish Laboratory, 19 J. J. Thomson Avenue, Cambridge CB3 0HE, UK
[16] Institute of Space Sciences (ICE-CSIC), Campus UAB, Carrer de Can Magrans, s/n, E-08193 Barcelona, Spain
[17] Institut d'Estudis Espacials de Catalunya (IEEC), E-08034 Barcelona, Spain
[18] Astronomical Observatory, University of Warsaw, Al. Ujazdowskie 4, 00-478 Warszawa, Poland
[19] Las Cumbres Observatory, 6740 Cortona Drive, Suite 102, Goleta, CA 93117-5575, USA
[20] Department of Physics, University of California, Santa Barbara, CA 93106-9530, USA
[21] Cardiff Hub for Astrophysics Research and Technology, School of Physics & Astronomy, Cardiff University, Queens Buildings, The Parade, Cardiff, CF24 3AA, UK
[22] Department of Astrophysics/IMAPP, Radboud University, P.O. Box 9010, 6500 GL Nijmegen, The Netherlands
[23] SRON, Netherlands Institute for Space Research, Niels Bohrweg 4, 2333 CA Leiden, The Netherlands
[24] Instituto de Estudios Astrofísicos, Facultad de Ingeniería y Ciencias, Universidad Diego Portales, Av. Ejército Libertador 441, Santiago, Chile
[25] DTU Space, National Space Institute, Technical University of Denmark, Elektrovej 327, DK-2800 Kgs. Lyngby, Denmark
[26] Space Telescope Science Institute, Baltimore, MD 21218, USA
[27] Department of Physics and Astronomy, The Johns Hopkins University, Baltimore, MD 21218, USA
[28] Department of Astronomy, The Ohio State University, 140 West 18th Avenue, Columbus, OH, USA
[29] Department of Physics, The Ohio State University, 191 West Woodruff Avenue, Columbus, OH, USA
[30] Center for Cosmology and Astroparticle Physics, The Ohio State University, 191 West Woodruff Avenue, Columbus, OH, USA
[31] Konkoly Observatory, CSFK, MTA Centre of Excellence, Konkoly Thege M. út 15-17, Budapest, 1121, Hungary
[32] ELTE Eötvös Loránd University, Institute of Physics and Astronomy, Pázmány Péter sétány 1/A, Budapest, 1117 Hungary
[33] Department of Experimental Physics, University of Szeged, Dóm tér 9, Szeged, 6720, Hungary
[34] Department of Astronomy, University of Texas at Austin, 2515 Speedway Stop C1400, Austin, TX 78712-1205, USA
[35] School of Physics and Astronomy, University of Southampton, Southampton, SO17 1BJ, UK
Received 2023 July 5; revised 2023 August 9; accepted 2023 August 14; published 2023 September 1

Abstract

We present the discovery and extensive follow-up of a remarkable fast-evolving optical transient, AT 2022aedm, detected by the Asteroid Terrestrial impact Last Alert Survey (ATLAS). In the ATLAS *o* band, AT 2022aedm exhibited a rise time of 9 ± 1 days, reaching a luminous peak with $M_g \approx -22$ mag. It faded by 2 mag in the *g* band during the next 15 days. These timescales are consistent with other rapidly evolving transients, though the luminosity is extreme. Most surprisingly, the host galaxy is a massive elliptical with negligible current star formation. Radio and X-ray observations rule out a relativistic AT 2018cow–like explosion. A spectrum in the first few days after explosion showed short-lived He II emission resembling young core-collapse supernovae, but

[36] CCAPP Fellow.

obvious broad supernova features never developed; later spectra showed only a fast-cooling continuum and narrow, blueshifted absorption lines, possibly arising in a wind with $v \approx 2700$ km s^{-1}. We identify two further transients in the literature (Dougie in particular, as well as AT 2020bot) that share similarities in their luminosities, timescales, color evolution, and largely featureless spectra and propose that these may constitute a new class of transients: luminous fast coolers. All three events occurred in passive galaxies at offsets of ∼4–10 kpc from the nucleus, posing a challenge for progenitor models involving massive stars or black holes. The light curves and spectra appear to be consistent with shock breakout emission, though this mechanism is usually associated with core-collapse supernovae. The encounter of a star with a stellar-mass black hole may provide a promising alternative explanation.

Unified Astronomy Thesaurus concepts: Transient sources (1851); Supernovae (1668); Tidal disruption (1696)

Supporting material: data behind figure

1. Introduction

Astrophysical transients are now found in the thousands by optical time-domain surveys with wide-field robotic telescopes, such as the Asteroid Terrestrial impact Last Alert System (ATLAS; Tonry et al. 2018), Panoramic Survey Telescope and Rapid Response System (Pan-STARRS; Chambers et al. 2016), Zwicky Transient Facility (ZTF; Bellm et al. 2019), and All-sky Automated Search for Supernovae (Shappee et al. 2014). These are unearthing a variety of new phenomena, and survey power is now set to increase even further with the Rubin Observatory, the first wide-field survey on an 8 m class telescope (Ivezić et al. 2019).

Improvements in survey cadence allow us to probe populations of transients that rise and fade on timescales of days, compared to the weeks–months of typical supernovae (SNe). The majority of fast transients seem to arise from stripped massive stars (Ho et al. 2023). These include the initial cooling peaks of Type IIb SNe, as well as events strongly interacting with a dense circumstellar medium (CSM) deficient in hydrogen (SNe Ibn; Pastorello et al. 2007; Hosseinzadeh et al. 2017) and sometimes helium (SNe Icn; Fraser et al. 2021; Gal-Yam et al. 2022; Perley et al. 2022).

A more mysterious population of fast transients has also been uncovered, with blue colors and a wide range of peak luminosities up to $M < -20$ mag, approaching superluminous SNe (SLSNe; Quimby et al. 2011; Gal-Yam 2019). Since their identification in Pan-STARRS1 (PS1) by Drout et al. (2014), such objects have been discovered in data from the Palomar Transient Factory and the Supernova Legacy Survey (Arcavi et al. 2016), the Dark Energy Survey (DES; Pursiainen et al. 2018), ATLAS (Prentice et al. 2018), Kepler (Rest et al. 2018), Hyper Suprime Cam (HSC; Tampo et al. 2020; Jiang et al. 2022) and ZTF (Ho et al. 2023). They have been termed fast blue optical transients or rapidly evolving transients (RETs). Their association with star-forming galaxies suggests a connection with massive stars (Wiseman et al. 2020), and their photometric evolution appears consistent with shock breakout from a dense, extended envelope (Drout et al. 2014; Pursiainen et al. 2018).

Several of the best-observed RETs also show persistent high temperatures and luminous X-ray and radio emission. The most famous example is AT 2018cow (Margutti et al. 2019; Perley et al. 2019; Prentice et al. 2019), but other well-studied objects include CSS 161010 (Coppejans et al. 2020), AT 2018lug (Ho et al. 2020), AT 2020xnd (Perley et al. 2021; Bright et al. 2022; Ho et al. 2022), and AT 2020mrf (Yao et al. 2022). These "Cow-like" events seem to be energized by continuous injection from a central engine (Margutti et al. 2019), though interaction with CSM can also contribute luminosity (Ho et al. 2020). Tidal disruption events (TDEs) of stars by intermediate-mass black holes (BHs) have been considered as an alternative model (Perley et al. 2019), though accretion onto a stellar-mass BH following the collapse of a massive star appears to be favored by most authors (e.g., Coppejans et al. 2020; Perley et al. 2021; Gottlieb et al. 2022).

Here we present an extraordinary new rapid transient that points to a distinct class of luminous, fast-cooling events. Object AT 2022aedm, or ATLAS 22bonw, was discovered by ATLAS on 2022 December 30 (Tonry et al. 2022). Spectroscopy carried out the following day by the Advanced Public ESO Spectroscopic Survey of Transient Objects (ePESSTO+; Smartt et al. 2015) suggested a likely SN, though of indeterminate spectral type (Gkini et al. 2022). A spectroscopic host galaxy redshift $z = 0.14343$ from the Sloan Digital Sky Survey (SDSS; Albareti et al. 2017) indicated a peak absolute magnitude $M_o = -21.5$ mag,[37] but the rising light curve was faster than any known SLSN. A relatively featureless spectrum and, most surprisingly, an elliptical host galaxy further added to the intrigue of this event, motivating extensive follow-up observations.

2. Observations

2.1. Ground-based Imaging

The object AT 2022aedm was discovered in the ATLAS transient stream processed by the ATLAS Transient Science Server (Smith et al. 2020). Calibrated ATLAS data in the cyan (c) and orange (o) bands were obtained using the ATLAS forced photometry service (Tonry et al. 2018; Smith et al. 2020; Shingles et al. 2021). ATLAS typically obtains four exposures per night in a given band; we combined each quad into a single average flux measurement to improve the signal-to-noise ratio. After AT 2022aedm had faded below $o \sim 19$ mag, observations were binned over neighboring nights to improve the signal-to-noise ratio.

Follow-up photometry was obtained from Pan-STARRS in the i, z, and y bands; the Las Cumbres Observatory (LCO) global telescope network (as part of the Global Supernova Project) in the B, g, V, r, and i bands; and the Liverpool Telescope (LT) in the u, g, r, i, and z bands. Data from the European Southern Observatory New Technology Telescope (NTT) were obtained using both EFOSC2 for the optical g, r, i, and z bands and SOFI for the near-infrared (NIR) J, H, and K

[37] We assume a flat ΛCDM cosmology with $H_0 = 70$ km s^{-1} Mpc^{-1} and $\Omega_\Lambda = 0.7$, giving a luminosity distance $D_L = 679$ Mpc and a Galactic extinction $E(B-V) = 0.0428$ for this line of sight (Schlafly & Finkbeiner 2011).

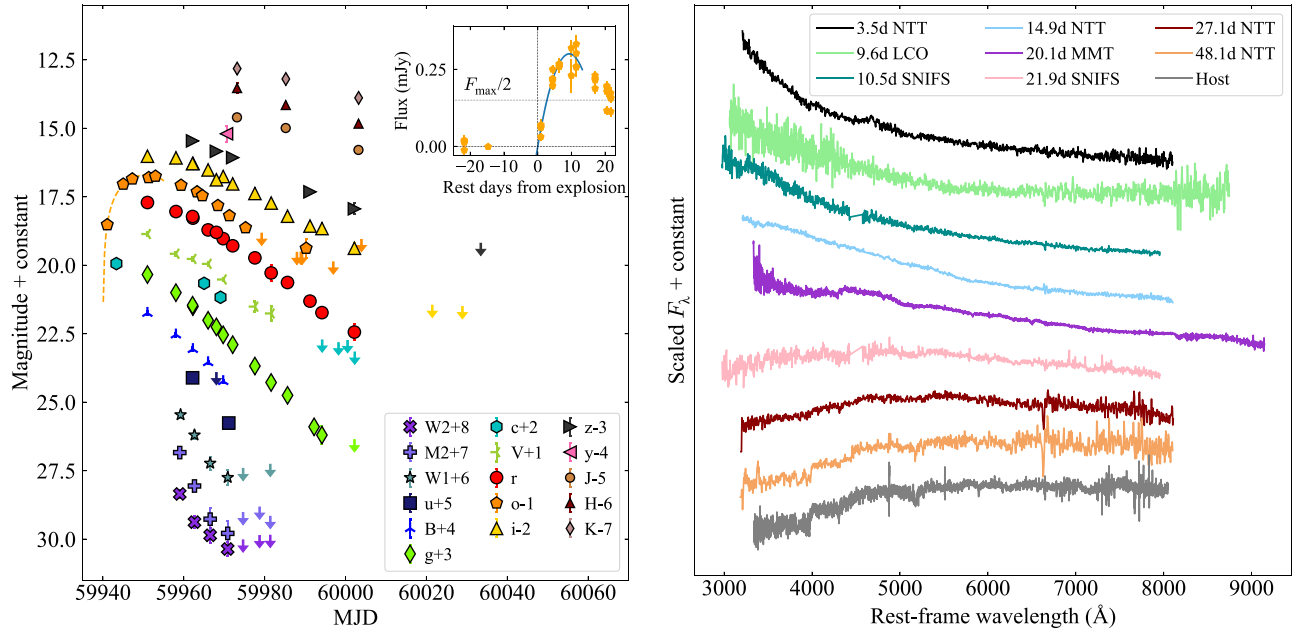

Figure 1. Follow-up of AT 2022aedm. Left: multicolor light curves from UV to NIR. Arrows indicate upper limits. The inset shows the early ATLAS flux data with a second-order fit (also shown on the multicolor plot) and time above half-maximum. Taking the shallowest and steepest rises allowed by the ATLAS data changes the time of zero flux by $\lesssim$0.5 days. Right: spectroscopic follow-up. Spectra are labeled by telescope/instrument and time since explosion in the rest frame. The photometric data shown on the left are available as the data behind the figure.

(The data used to create this figure are available.)

bands as part of ePESSTO+. The data were reduced (debiased and flat-fielded) either automatically by facility pipelines or manually using the PESSTO pipeline (Smartt et al. 2015) in the case of the NTT data.

2.2. Photometry Sans Frustration

Photometry was performed using a custom pipeline, Photometry Sans Frustration (or PSF).[38] This is a fully PYTHON-based code employing aperture and point-spread function (PSF) fitting photometry routines from ASTROPY (Astropy Collaboration et al. 2013, 2018) and PHOTUTILS (Bradley et al. 2020). As well as deriving the image background, PSF, and zero-point, the code provides options to automatically download local star catalogs and reference images using ASTROQUERY (Ginsburg et al. 2019), solve the coordinate system using ASTROMETRY.NET (Lang et al. 2010), clean cosmic rays using LACOSMIC (van Dokkum et al. 2012), align and stack images using ASTROALIGN (Beroiz et al. 2020), and subtract transient-free reference images of the field using PYZOGY (Zackay et al. 2016; Guevel & Hosseinzadeh 2017).

All NTT, LCO, and LT images were first cleaned and stacked within each night. Calibration stars and template images were obtained in *g*, *r*, *i*, and *z* from Pan-STARRS (Flewelling et al. 2020); *u* from the SDSS; and *J*, *H*, and *K* from the VISTA Kilo-degree Galaxy Survey (Edge et al. 2013). The LCO *B* and *V* reference images were obtained after the transient faded. The PSF for each science and template image was determined using the local reference stars. All transient fluxes were measured after template subtraction to remove host galaxy light. The full photometric data set is shown in Figure 1.

[38] https://github.com/mnicholl/photometry-sans-frustration

2.3. Swift Observations

We obtained ultraviolet (UV) and X-ray data using target-of-opportunity observations with the UV-Optical Telescope (UVOT; Roming et al. 2005) and X-ray Telescope (XRT; Burrows et al. 2005) on board the Neil Gehrels Swift Observatory (Swift; Gehrels et al. 2004). The UVOT imaging was carried out in the *uvw*2, *uvm*2, and *uvw*1 filters. The light curves were measured using a 5″ aperture. Count rates were obtained using the Swift UVOTSOURCE tools and converted to magnitudes (in the AB system) using the UVOT photometric zero-points (Breeveld et al. 2011). No host subtraction was performed in the UV bands, as host contamination is negligible at these wavelengths (this is confirmed by the later UVOT visits that only result in nondetections).

We processed the XRT data using the online analysis tools provided by the UK Swift Science Data Centre (Evans et al. 2007, 2009). Object AT 2022aedm is not detected in the combined 15.3 ks exposure, with a limiting count rate $<8.53\times10^{-4}$ s^{-1}. Assuming a power-law spectrum with $\Gamma=2$ (Coppejans et al. 2020) and a Galactic hydrogen column density toward AT 2022aedm of 4.2×10^{20} cm^{-2} (HI4PI Collaboration et al. 2016), this corresponds to an unabsorbed 0.3–10 keV luminosity $L_X<3.8\times10^{42}$ erg s^{-1}. This upper limit is deeper than the observed X-ray luminosities of $\sim10^{43-44}$ erg s^{-1} in AT 2018cow (Margutti et al. 2019), AT 2020xnd (Ho et al. 2022), and AT 2022tsd (Matthews et al. 2023).

2.4. Radio Observations

We observed AT 2022aedm with the Arcminute Microkelvin Imager–Large Array (AMI–LA; Zwart et al. 2008; Hickish et al. 2018) over 4 epochs beginning 20 days after discovery. The AMI–LA is an eight-dish interferometer based in

Cambridge, UK. Each dish is 12.8 m in diameter, enabling an angular resolution of $\sim 30''$. The facility observes at a central frequency of 15.5 GHz with a bandwidth of 5 GHz.

Data taken with AMI–LA were reduced using a custom pipeline, REDUCE_DC. We used 3C 286 and J1119+0410 as the primary and secondary calibrators, respectively, to perform amplitude and phase calibration. The pipeline also flags the data for radio-frequency interference, effects of poor weather, and antenna shadowing. The data were then exported in *uvfits* format ready for imaging.

Further flagging and imaging were conducted in the Common Astronomy Software Applications (CASA, Version 4.7.0; McMullin et al. 2007; CASA Team et al. 2022) using the tasks *tfcrop*, *rflag*, and *clean*. Object AT 2022aedm is not detected in any of the final images, with 3σ upper limits of $F_\nu < [41, 210, 156, 96]$ μJy at 20, 66, 107, and 110 days after the first optical detection. These correspond to limits on the spectral luminosity of $L_\nu < 2.3 \times 10^{28}$–$1.2 \times 10^{29}$ erg s^{-1} Hz^{-1}. For comparison, Cow-like RETs typically exhibit radio emission at the level of $L_\nu \gtrsim 10^{29}$ erg s^{-1} Hz^{-1} (at $\sim$10 GHz) on timescales of months (Coppejans et al. 2020; Ho et al. 2020).

2.5. Spectroscopy

We obtained optical spectra of AT 2022aedm using EFOSC2 on the NTT (through ePESSTO+), the LCO 2 m telescopes, the SuperNova Integral Field Spectrograph (Lantz et al. 2004; Tucker et al. 2022) on the University of Hawaii 2.2 m telescope, and Binospec on the 6.5 m MMT (Fabricant et al. 2019). Spectroscopy from ePESSTO+ commenced on 2022 December 31 (within a day after the object was flagged by ATLAS) and continued until 2023 February 20, by which time the spectrum was indistinguishable from a preexplosion host galaxy spectrum from SDSS.

Standard reductions of these data, including debiasing, flat-fielding, spectral extraction, and flux and wavelength calibration, were performed using instrument-specific pipelines. The reduced spectra are plotted in Figure 1 and labeled with the instrument and phase with respect to our estimated explosion date. We assume that host galaxy extinction is negligible, supported by the lack of Na I D absorption in these spectra (Poznanski et al. 2012) and the early blue colors in our spectra and photometry. All data will be made publicly available via WISeREP (Yaron & Gal-Yam 2012).

3. Analysis

3.1. Light Curve

The rising light curve of AT 2022aedm is well constrained by the early ATLAS *o*-band detections. The discovery point on MJD 59,941.1 at $o = 19.51$ mag is a factor of $\simeq$5 below the peak *o*-band flux. Fitting a second-order polynomial to the early flux light curve (Figure 1) indicates the explosion occurred on MJD $59{,}940.0 \pm 0.5$ ($\approx$1 day before the first detection), reaching the *o*-band peak on MJD $59{,}950.6 \pm 0.5$. We take these as the dates of explosion and peak throughout. We note, however, that the last nondetection is 15 days before detection, so a slightly earlier explosion date cannot be entirely ruled out if the early light-curve shape is more complex. The rest-frame rise time from half the peak flux is $t_{r,1/2} = 6.6$ days, much shorter than the SLSNe that reach comparable peak luminosities but with $t_{r,1/2} = 10$–40 days (Nicholl et al. 2015; De Cia et al. 2018; Lunnan et al. 2018).

The fading timescale of AT 2022aedm is also much quicker than most other luminous transients. The *g*-band light curve fades by 2 mag in the 15 days after peak, and by 18 days, it has declined to 10% of the peak *g*-band flux. In the *o* band, where we also have the rise, the FWHM (i.e., the total time spent within 50% of peak flux) is $t_{1/2} = 19 \pm 1$ days. These timescales are well within the distributions measured for RETs discovered in the DES (Pursiainen et al. 2018). Although the measured $t_{1/2}$ for AT 2022aedm is longer than the $t_{1/2} < 12$ days defining RETS in PS1 (Drout et al. 2014) and ZTF (Ho et al. 2023), this is attributable to using different photometric filters; we measured $t_{1/2}$ in *o*, where the rate of fading in AT 2022aedm is $\approx$55% slower than in the *g* band. Correcting by this factor gives an estimated *g*-band $t_{1/2}$ of $\approx$12 days.

The extinction-corrected *g*-band peak luminosity of AT 2022aedm, $M_g = -22.04 \pm 0.05$, makes it one of the brightest RETs discovered to date. It outshines all but one event (DES 16E1bir) in the combined PS1+DES+ZTF sample. The closest spectroscopically classified RETs in terms of luminosity are the Cow-like RETs, typically reaching ≈ -21 mag (Ho et al. 2023). To highlight the exceptional luminosity of AT 2022aedm, we show a combined *g*- and *c*-band rest-frame light curve in Figure 2, compared to representative examples of different types of fast-fading transients. Object AT 2022aedm is broader and brighter than AT 2018cow but fades faster than the fastest SLSN, SN 2018bgv (Chen et al. 2023). It is much more luminous than a typical RET (Drout et al. 2014); the fastest TDE, AT 2020neh (Angus et al. 2022); the fastest broad-lined SNe Ic, such as iPTF16asu (Whitesides et al. 2017; see also SN 2018gep and SN 2018fcg; Pritchard et al. 2021; Gomez et al. 2022); or any fast interacting transients of Types IIn (Ofek et al. 2010), Ibn (Hosseinzadeh et al. 2017), or Icn (Fraser et al. 2021; Perley et al. 2022).

Figure 2 also shows the $g - r$ (or $B - V$) color evolution of AT 2022aedm compared to the same sample of objects (where multiple bands are available). From an initial $g - r = -0.37$ at 10 days after explosion, AT 2022aedm dramatically reddens by 1.8 mag in color index over the next 35 rest-frame days. Cow-like RETs, TDEs, and interacting transients generally show a more gradual or flat color evolution. The color change in AT 2022aedm is more consistent with events with expanding, cooling photospheres; it lies intermediate between iPTF 16asu and SN 2018bgv. Object PS1-10bjp shows a similar color evolution over the first 10 days.

Two unclassified fast transients show a comparable color evolution in combination with a peak absolute magnitude brighter than -20 mag. One is AT 2020bot, the only RET in the ZTF sample that did not fit into any of the stripped-envelope, interacting, or Cow-like subpopulations (Ho et al. 2023). It is fainter than AT 2022aedm, with a faster rise and redder average color. A stronger similarity is exhibited by "Dougie" (Vinkó et al. 2015), a mysterious transient discovered by ROTSE in 2009. This event peaked at -22.5 mag after a fast rise of $\approx$10 days. The early light-curve shape is very similar to that of AT 2022aedm, though the decline may flatten after 30–40 days. However, this flattening could also be due to a host contribution in its UVOT photometry. While the light curve could be plausibly interpreted as a super-Eddington TDE (Vinkó et al. 2015), its position offset from the host nucleus and lack of distinct spectroscopic features make this classification far from certain.

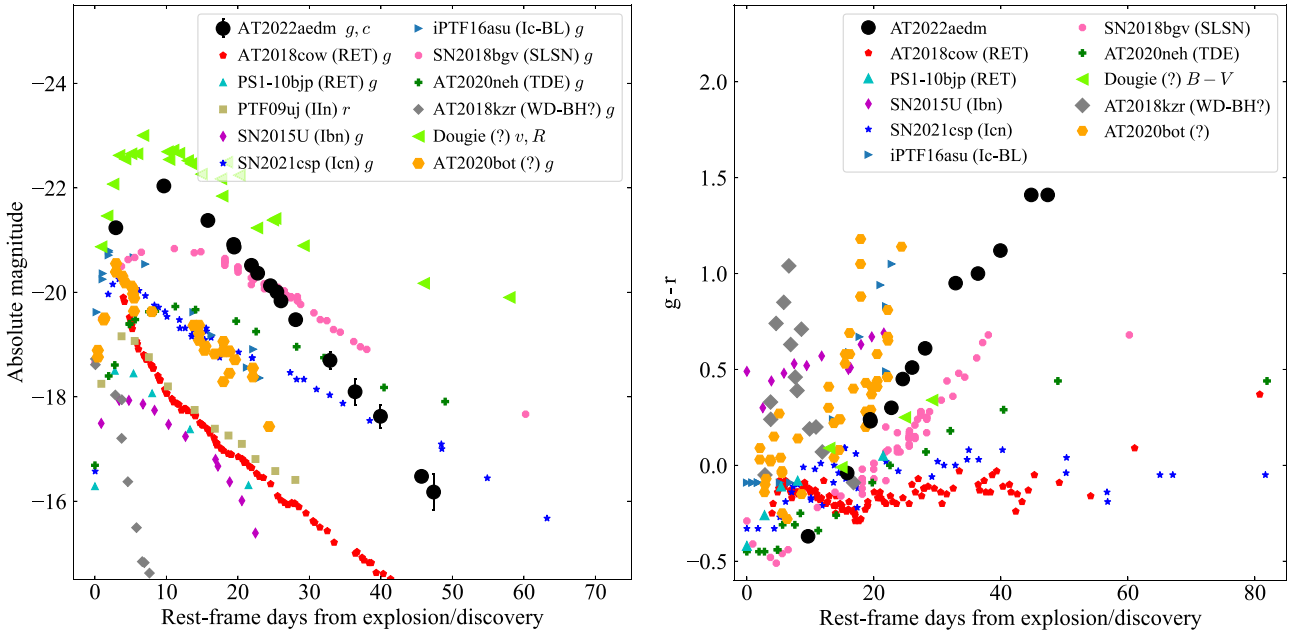

Figure 2. Photometric comparison of AT 2022aedm and other fast transients. For visual clarity, we plot the uncertainties only for AT 2022aedm. Left: absolute rest-frame light curves. Right: $g-r$ color evolution.

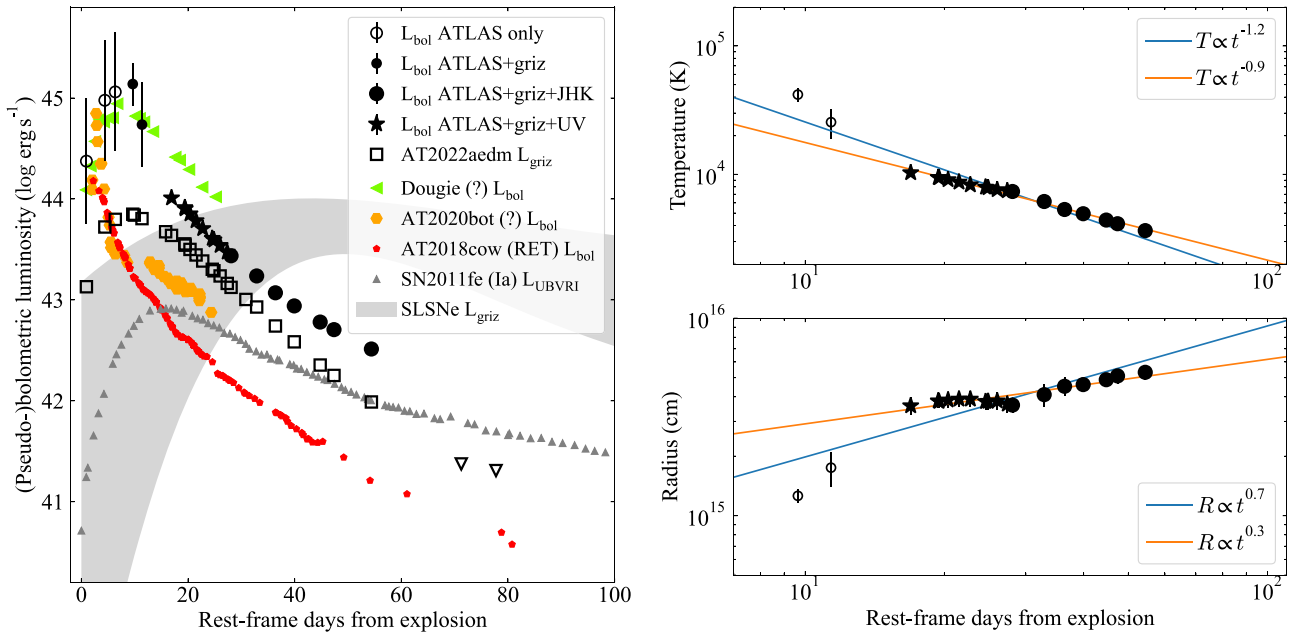

Figure 3. Results from fitting the multiband photometry with SUPERBOL. Left: bolometric and pseudobolometric (optical) light curves compared to AT 2018cow, AT 2020bot, and Dougie. We also show a representative SN Ia (Nugent et al. 2011) and an SLSN sample (Nicholl et al. 2015). For visual clarity, we plot the uncertainties only for AT 2022aedm. Right: temperature and radius evolution from blackbody fits, together with the best-fitting power laws. The orange lines are not fit to the first two data points, for which no UV or NIR data are available.

3.2. Bolometric Light Curve

To measure the overall energetics of AT 2022aedm, we integrate our multiband photometry using SUPERBOL (Nicholl 2018). We construct a pseudobolometric light curve using the excellent g-, r-, i-, z-, and o-band coverage and estimate the full bolometric light curve by fitting blackbody functions to these bands and our UV and NIR photometry where available. These light curves are shown in Figure 3.

The peak pseudobolometric luminosity is typical of SLSNe, reaching $L_{griz} = 10^{43.8}$ erg s^{-1}, but the light-curve rise and decline rates fall well outside the SLSN distribution. The decay rate is comparable to AT 2018cow, though the rise is longer than the <2 days exhibited by that event. The estimated full bolometric luminosity of AT 2022aedm at peak is exceptionally high, reaching $\approx 10^{45}$ erg s^{-1}. This is due to a high temperature, $T \gtrsim 30{,}000$ K (shown in the top right panel), suggested by the very blue $g-r$ and $r-i$ colors in the first LCO images. The temperature exhibits a monotonic decline with a scaling of roughly $T \propto 1/t$. The blackbody radius increases throughout our observations, suggestive of an expanding photosphere that remains optically thick. The estimated bolometric light curves of Dougie and AT 2020bot,

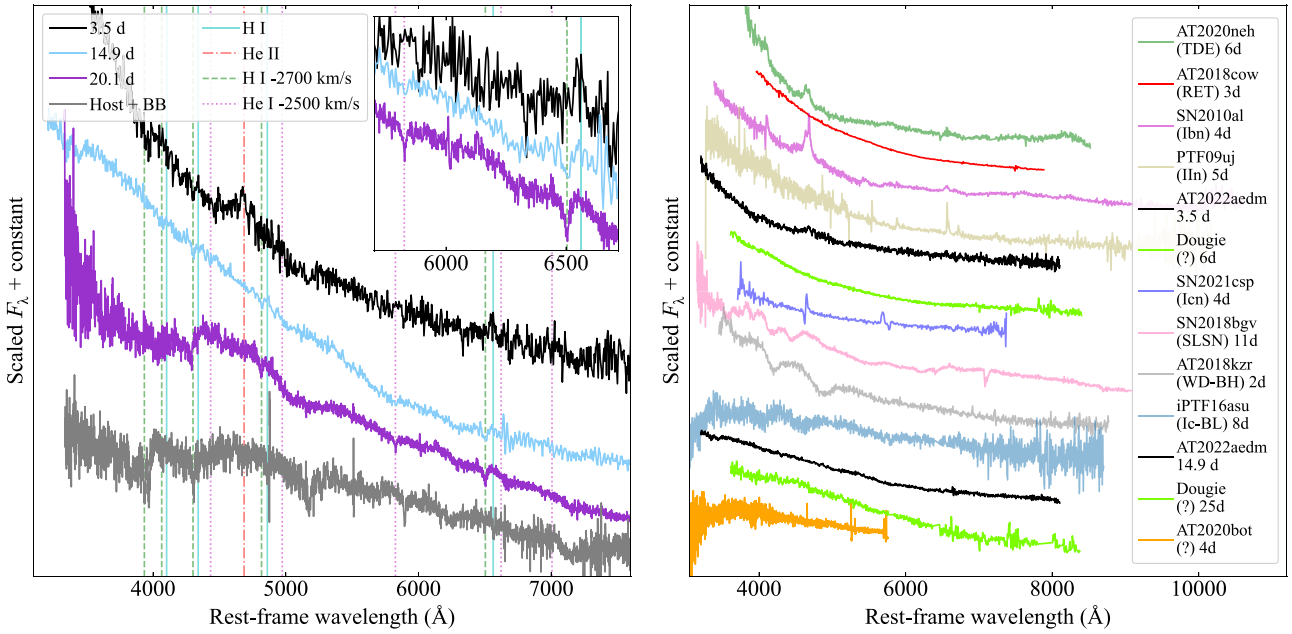

Figure 4. Spectroscopic analysis of AT 2022aedm. Left: line identification in the highest signal-to-noise ratio spectra. No unambiguous broad features are identified, but we clearly detect early emission lines of Hα and He II and, at later times, blueshifted absorption lines of H and He I. Right: comparison of AT 2022aedm with other fast transients. Dougie and AT 2020bot also show a lack of obvious SN features and occurred in similar environments to AT 2022aedm.

also constructed using SUPERBOL, peak at similar luminosities to AT 2022aedm.

3.3. Spectra

The spectroscopic evolution of AT 2022aedm is shown in Figure 1. The cooling observed in the photometry is also evident in its spectra. The first NTT spectrum 3.5 days after explosion shows a strong blue continuum, which weakens and disappears by day 27. By day 48, the spectrum is indistinguishable from an archival SDSS spectrum of the host galaxy.

The spectra mostly lack the obvious broad emission, absorption, or P Cygni lines typically seen in SNe. The spectra on days 3 and 14 (both from NTT) and 20 (from MMT) with the best signal-to-noise ratios are examined in more detail in Figure 4. Weak broad features may exist at around 4000–5000 Å after day 20, though these could also be caused by contamination from the host galaxy, which is around 2 mag brighter than AT 2022aedm at this phase. We show this explicitly by adding an arbitrary 20,000 K blackbody to the host, finding that this reasonably reproduces the overall shape of the day 20 spectrum.

Figure 4 does show several narrow spectral lines of a clearly transient nature. The day 3 spectrum shows a sharply peaked emission line consistent with He II λ4686, possibly with a broader base. This line is often observed in very young SNe (Gal-Yam et al. 2014; Khazov et al. 2016; Bruch et al. 2021) and in TDEs (Gezari et al. 2012; Arcavi et al. 2014) due to the high radiation temperatures capable of ionizing helium. We also detect a weak narrow Hα emission line. Other Balmer lines are not visible at this signal-to-noise ratio. The He II is not detected in any later spectra, likely because the temperature has fallen too low to maintain helium ionization.

The spectra on days 14 and 20 show narrow absorption, rather than emission, from hydrogen and neutral helium. The first three transitions of the Balmer series are clearly visible but blueshifted from their rest wavelengths by $\approx$2700 km s^{-1}. The high-resolution MMT/Binospec data on day 20 also clearly show He I λ5875 absorption blueshifted by $\approx$2500 km s^{-1}. These lines are not visible in the host spectrum, confirming their association with the transient.

Figure 4 also includes a comparison between the early spectra of AT 2022aedm and other fast transients. The initial He II and Hα emission is reminiscent of some SNe Ibn (Hosseinzadeh et al. 2017), as well as the fast-evolving TDE AT 2020neh (Angus et al. 2022). The earliest spectrum is also a reasonable match for young SNe IIn, including the shock breakout candidate PT 09uj (Ofek et al. 2010). However, AT 2022aedm never develops the strong emission lines typically seen in these classes at later times. The largely featureless spectrum even at 15 days is a poor match for any fast-evolving SNe Ic, SLSNe, or SNe Icn.

Cow-like RETs exhibit quite featureless spectra at peak, but the prototype AT 2018cow showed increasingly clear H and He emission lines as it evolved, the opposite of the case in AT 2022aedm. Interestingly, the spectra of Dougie remained featureless for $\gtrsim$30 days (Vinkó et al. 2015) and seemed to cool in a manner similar to AT 2022aedm. Object AT 2020bot lacks a full spectroscopic time series, making a detailed comparison difficult. It shows an unusual spectrum at maximum light. Ho et al. (2023) noted the presence of possible broad features, weak compared to typical SN lines and without an obvious identification. In Section 3.1, we observed that these two events also shared some key photometric properties with AT 2022aedm.

3.4. Host Galaxy

The host galaxy of AT 2022aedm is LEDA 1245338 (or SDSS J111927.73+030632.7). This is a bright, red galaxy with $M_r = -22.8$ mag; Figure 5 illustrates this with a color image obtained from Pan-STARRS. An SDSS spectrum is also available (shown in Figure 4). Both the SDSS spectral fitting

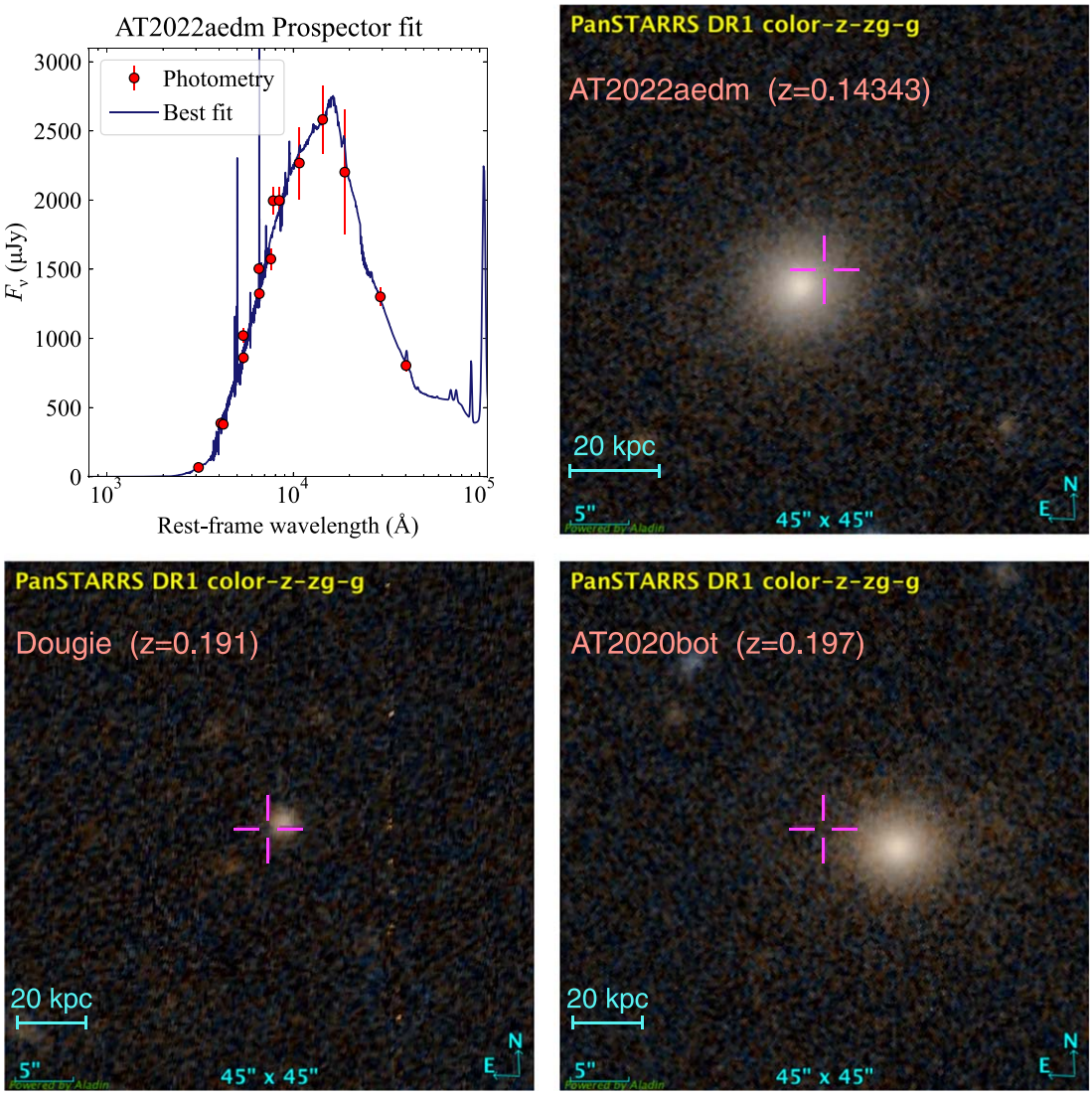

Figure 5. Top left: fit to the AT 2022aedm host galaxy SED using PROSPECTOR. Top right: host galaxy color image. Bottom row: elliptical host galaxies and offsets of two other luminous fast-cooling transients with unusual spectra (Vinkó et al. 2015; Ho et al. 2023). Images are from Pan-STARRS and centered at the transient positions.

and Galaxy Zoo morphological analysis classify LEDA 1245338 as an elliptical galaxy.

The SDSS data release also includes an automated analysis of the SDSS spectrum with the Portsmouth pipeline (using the method of Maraston et al. 2009). The spectral fitting measures a total stellar mass of $\approx 10^{11.5}\ M_\odot$ and a star formation rate (SFR) consistent with zero. They find a mean age of the stellar population of 4.8 Gyr. Given that spectral energy distribution (SED) modeling is highly sensitive to the assumed functional form of the star formation history (Carnall et al. 2019; Leja et al. 2019), we run our own analysis of the host photometry over a wider wavelength range using PROSPECTOR (Johnson et al. 2021). In particular, we use the PROSPECTOR-α model employing a nonparametric star formation history, with six equal-mass star-forming bins of flexible width (see Leja et al. 2017, for details). We include archival host photometry from SDSS, the Two Micron All Sky Survey (Skrutskie et al. 2006), and the Wide-field Infrared Survey Explorer (Wright et al. 2010). The fit is shown in Figure 5. We measure $M_* = 10^{11.45}\ M_\odot$, consistent with the SDSS results, and a specific SFR (sSFR) in the last 50 Myr of $\log(\mathrm{sSFR}/\mathrm{yr}^{-1}) = -11.69$.

The SDSS analyses and our PROSPECTOR results confirm that the host of AT 2022aedm is a massive "red and dead" galaxy. This is surprising; recent work by Irani et al. (2022) shows that less than 1% of core-collapse explosions occur in such environments. Moreover, this galaxy is especially unlike the hosts of most transients with comparable luminosity. The SLSNe occur almost exclusively in low-mass galaxies with $<10^{10}\ M_\odot$ (Lunnan et al. 2014; Leloudas et al. 2015; Perley et al. 2016; Chen et al. 2017; Schulze et al. 2018), and their average sSFR is 3 orders of magnitude greater than our measurement for AT 2022aedm. Bright RETs are also found in relatively low-mass, star-forming host galaxies; the sSFRs of the RET hosts in PS1 and DES span $-10 \lesssim \log(\mathrm{sSFR}/\mathrm{yr}^{-1}) \lesssim -8$, with only three (out of 73) fitting best to a passive galaxy model and only two having a stellar mass greater than $10^{11} M_\odot$. Wiseman et al. (2020) conducted a systematic analysis of RET hosts in DES, finding evidence for star formation in all of the 49 galaxies for which redshifts were available, and the five RETs from HSC were also found in star-forming galaxies (Tampo et al. 2020).

Notably, two other fast transients from our photometric and spectroscopic comparisons also occurred in elliptical galaxies: Dougie and AT 2020bot (Vinkó et al. 2015; Ho et al. 2023). The Pan-STARRS images of their hosts are shown alongside AT 2022aedm in Figure 5. We also note that one SN Ibn, PS1-12sk, exploded in a bright elliptical, prompting Hosseinzadeh et al. (2019) to suggest that not all SNe Ibn result from massive stars.

4. Discussion

4.1. A New Class of Transient?

Object AT 2022aedm is a puzzling event with a very unusual set of properties:

1. a high peak luminosity in the optical, with $M_g \approx -22$ mag;
2. no luminous radio or X-ray emission;
3. fast rise and decline rates, fading $\sim$1 mag week^{-1} in the g band;
4. rapid cooling from $\sim$30,000 to $\sim$4000 K in a few weeks following peak;
5. a spectrum dominated by a smooth continuum with no high equivalent width absorption or emission lines at any phase; and
6. a massive host galaxy comprised of an old stellar population, with no evidence for current star formation.

This combination is not consistent with any known class of transients. An extensive search of the literature reveals two other objects that share the key properties: $M < -20$ mag, rise time <10 days, fast decline and color evolution, and weak spectroscopic features at all times. Together, these events indicate a new class of fast transients with high optical luminosities and fast cooling after peak. Dougie (Vinkó et al. 2015) in particular shows a strong photometric and spectroscopic similarity, while AT 2022bot (Ho et al. 2023) may represent an even faster-evolving member of this class. All three occurred off-center within passive host galaxies, indicating that—uniquely among RETs—these new "luminous fast coolers" (LFCs) do not require young stellar populations.

4.2. Rates

We estimate the volumetric rate of these events using the ATLAS Survey Simulator (McBrien 2021; Srivastav et al. 2022). Interpolated absolute light curves of AT 2022aedm in the c and o bands are inserted into the simulation at 10,000 random times, positions, and redshifts (up to some $z_{\rm max}$) and compared to the cadence, footprint, and depth of the true ATLAS survey to determine the number of 5σ detections of each injected event.

We define a discovery as those objects detected in more than $n_{\rm det}$ images (or $\approx n_{\rm det}/4$ nights, since ATLAS typically obtains a quad of exposures per night at a given pointing). We then take all real transients brighter in apparent magnitude than the injected transient at $z = z_{\rm max}$ and having at least the same number of ATLAS detections and take as our spectroscopic completeness the fraction of these transients that were classified. The rate is then

$$R = \frac{N_{\rm events}}{f_{\rm disc}\, f_{\rm spec} \int_0^{z_{\rm max}} T \Big/ (1+z) \frac{dV}{dz} dz}, \quad (1)$$

where $T = 2.5$ yr is the duration of the mock survey (with the factor $1/(1+z)$ accounting for time dilation over the observed redshift range), dV/dz is the differential comoving volume between redshift z and $z + dz$, $f_{\rm disc}$ and $f_{\rm spec}$ are the fractions discovered and classified, and $N_{\rm events} = 1$ is the number of observed AT 2022aedm–like transients in ATLAS.

We set $z_{\rm max} = 0.2$, covering the redshift range within which LFCs have been discovered, and set $n_{\rm det} = 20$. The latter is motivated by the modal number of detections for real ATLAS transients and, with observations on 5 nights, should also enable identification of the fast light-curve shape. Varying $n_{\rm det}$ leads to less than a factor of 2 variation in our derived rate due to a trade-off between $f_{\rm disc}$ and $f_{\rm spec}$; stricter requirements lead to a smaller discovered sample but with a higher spectroscopic completeness. For these parameters, our survey simulation returns $f_{\rm disc} = 0.35$ and $f_{\rm spec} = 0.58$, giving $R \approx 1$ Gpc^{-3} yr^{-1}.

We caution that this estimate applies to the brightest LFCs such as AT 2022aedm and Dougie, and that fainter and faster events such as AT 2020bot are likely more common volumetrically but harder to detect. Nevertheless, our derived rate indicates that these events are very rare, $\sim 10^{-5}$ of the core-collapse SN rate. This rate is lower than the SLSN rate of a few $\times$ 10 Gpc^{-3} yr^{-1} (Frohmaier et al. 2021) but may be consistent with the rate of Cow-like events, estimated as 0.3–420 Gpc^{-3} yr^{-1} (Ho et al. 2023).

4.3. Physical Scenarios for LFCs

4.3.1. Tidal Disruption Events

Vinkó et al. (2015) favored a TDE as the origin of Dougie. A model with a relatively low-mass BH of $\sim 10^5\ M_\odot$ provided a good match to the fast-evolving light curve. Although the host galaxy luminosity was more consistent with a central BH mass of $\sim 10^7\ M_\odot$, Dougie's location $\sim$4 kpc from the nucleus could indicate a disruption around a wandering intermediate-mass BH.

This scenario has difficulty accounting for AT 2022aedm. We are unable to find an acceptable fit using the TDE model in MOSFIT[39] (Guillochon et al. 2018; Mockler et al. 2019), where models cannot reproduce the steep decline from peak or the fast color evolution. The shallower decay of Dougie at late times may include some host contribution, causing a flattening that mimics the power-law decay of TDE models.

Other circumstantial problems arise in trying to explain LFCs as TDEs. Objects AT 2022aedm and AT 2020bot have even larger offsets from the nuclei of their hosts. In particular, AT 2020bot shows an offset of $\gtrsim$10 kpc in the outskirts of the galaxy, where the stellar density is low. This would make a TDE very unlikely (though at the available imaging depths, we cannot rule out a globular cluster). The TDE models would also need to explain why these offset events show such a strong evolution in color compared to TDEs in their host nuclei and are so much brighter than other TDEs with fast evolution (Blagorodnova et al. 2017; Nicholl et al. 2020; Angus et al. 2022; Charalampopoulos et al. 2023).

4.3.2. Nickel Powering and White Dwarf Explosions

Most SNe are heated by the decay of radioactive nickel (^{56}Ni) to cobalt and then iron, but this mechanism can be excluded for many of the known RETs (e.g., Drout et al. 2014; Pursiainen et al. 2018; Perley et al. 2021). The problem is that

[39] This is an updated version of the same model used to fit Dougie; see Guillochon et al. (2014).

fast light curves require low ejecta masses ($M_{\rm ej}$), while bright peak luminosities require large nickel masses ($M_{\rm Ni}$). Drout et al. (2014) showed that to produce a peak luminosity of $\sim 10^{44}$ erg and a rise time of <10 days, a nickel-powered model would need an ejecta velocity of $>0.1c$. We can probably rule out a very relativistic explosion in the case of AT 2022aedm due to our radio nondetections, though we cannot exclude a mildly relativistic expansion. More problematic is the requirement for $M_{\rm ej} \sim M_{\rm Ni} \sim 1\ M_\odot$. This would produce a spectrum dominated by iron-group absorption, very different from the blue and largely featureless spectra of LFCs at peak.

Despite the difficulties with a pure nickel-powered model, white dwarf progenitor models (i.e., variants of SNe Ia) would still be appealing to explain transients in old stellar populations. An SN Ia interacting with a dense CSM could produce a peak luminosity well in excess of typical SNe Ia without requiring $M_{\rm Ni} \sim M_{\rm ej}$. However, our NTT observations at 70–80 days after explosion indicate that AT 2022aedm had already faded below the luminosity of an SN Ia at the same epoch, making a hidden SN Ia unlikely. Moreover, known interacting SNe Ia produce spectra with strong, broad hydrogen emission and broad metal P Cygni lines (Silverman et al. 2013), very unlike the spectra of LFCs.

4.3.3. Magnetar Birth

Rapidly rotating nascent magnetars are suspected to play a role in many luminous and/or rapid transients, such as SLSNe, gamma-ray bursts, and fast radio bursts. Central engines are also thought to be required in the Cow-like RETs. Powering short-timescale, luminous events like LFCs would require a combination of rapid rotation to provide a large energy reservoir, a strong magnetic field to extract this energy quickly, and a low ejecta mass (e.g., Kasen & Bildsten 2010). We find that although the MOSFIT magnetar model (Nicholl et al. 2017) is able to adequately fit the decline phase of AT 2022aedm, it struggles to simultaneously match the fast rise, even with an ejecta mass $\lesssim 1\ M_\odot$.

The environments of known LFCs are also a major problem for this model. Long gamma-ray bursts and SLSNe are thought to prefer low-metallicity, star-forming galaxies because these are favorable for rapidly rotating core collapse. The massive elliptical hosts of LFCs are decidedly unfavorable. Less than 1% of core-collapse SNe occur in elliptical galaxies (Irani et al. 2022), and likely not all form magnetars. Kouveliotou et al. (1998) estimated that only $\sim$10% of core collapses form magnetars, though more recent work finds a potentially larger but rather uncertain fraction of $0.4^{+0.6}_{-0.28}$ (Beniamini et al. 2019). In any case, it appears unlikely that three unusual magnetar-forming explosions would all be found in elliptical galaxies. Moreover, the blueshifted narrow H and He lines in the later spectra of AT 2022aedm may indicate a dense wind preexplosion, which would strip angular momentum and inhibit magnetar formation.

4.3.4. Shock Breakout

Interaction with CSM is another mechanism thought to be responsible for many luminous or unusual transients, including (SL)SNe IIn, and fast events like SNe Ibn/Icn. Models for luminous SNe IIn generally invoke a massive CSM that releases energy slowly via postshock diffusion (Smith & McCray 2007). In the case of RETs, the more relevant models are shock breakout from an extended CSM or wind, which have been investigated by Chevalier & Irwin (2011) and Ginzburg & Balberg (2012). This model provided a reasonable explanation for the rapid SN IIn, PTF 09uj (Ofek et al. 2010), and other RETs (Drout et al. 2014). The early He II emission in AT 2022aedm is often seen during the shock breakout phase in normal Type II SNe (Gal-Yam et al. 2014; Bruch et al. 2023).

We apply the equations of Chevalier & Irwin (2011), following the prescriptions from Margutti et al. (2014), to estimate the ejecta and wind masses required in AT 2022aedm. We set the input parameters based on our SUPERBOL results: peak time $t_{\rm peak} = 8$ days, total radiated energy $E_{\rm rad} = 1.1 \times 10^{51}$ erg, and breakout radius $R_{\rm bo} \approx 2 \times 10^{15}$ cm. The equations are degenerate in $M_{\rm ej}/E^2$, where E is the kinetic energy of the explosion. We find $M_{\rm ej} = 0.02 (E/10^{51}{\rm erg})^2\ M_\odot$, with a wind density parameter[40] $D_* = 0.27$. For a wind velocity of 2700 km s^{-1}, based on the blueshifted absorption lines in the spectrum, this corresponds to a preexplosion mass-loss rate of $\dot{M} = 0.7\ M_\odot\ {\rm yr}^{-1}$.

Vinkó et al. (2015) noted that Dougie could also be explained by a reasonable shock-powered model, with an estimated $\approx 8 \times 10^{50}$ erg deposited in $\approx 2.6\ M_\odot$ of CSM, but disfavored this model based on the lack of shock-excited lines in the spectrum. It is shown by AT 2022aedm that emission lines can be very weak and short-lived in these events, perhaps making a CSM interpretation of Dougie more palatable. Nevertheless, the parameters we infer for AT 2022aedm (if shock breakout is the dominant power source) are difficult to associate with any specific progenitor. For a standard 10^{51} erg explosion, the low ejecta mass would be indicative of an ultrastripped SN, yet the wind is H- and He-rich, and the unsustainable high mass-loss rate would require that it is lost in the years immediately before explosion. For a very energetic explosion with 10^{52} erg, the implied ejecta mass is a more reasonable $\sim 2\ M_\odot$. But this large energy would likely require a massive progenitor, increasing the tension with the passive host galaxies of the LFCs.

4.4. Stellar-mass Compact Mergers

The old stellar populations hosting AT 2022aedm and other LFCs are more compatible with a compact object origin, rather than massive stars. However, we encountered inconsistencies in interpreting these objects as white dwarf explosions or TDEs from massive BHs. Fortunately, recent years have seen rapid progress in understanding the diversity of transients resulting from mergers involving neutron stars (NSs) and stellar-mass BHs, and we compare to such models here.

Kilonovae, transients powered by the decay of heavy elements ejected from NS mergers, have been discovered in targeted follow-up of gravitational waves (Abbott et al. 2017; Margutti & Chornock 2021) and gamma-ray bursts (Berger et al. 2013; Tanvir et al. 2013; Rastinejad et al. 2022). However, LFCs are much brighter and bluer than any plausible kilonovae, in which low ejecta masses of $<0.1\ M_\odot$ and large opacities conspire to produce faint red transients visible for only a few days in the optical. While no definitive detections exist, kilonovae from NS–BH mergers are expected to be even fainter and redder than those from binary NSs (Gompertz et al. 2023). Object AT 2018kzr was a so-far unique event suggested

[40] Defined as $D_* \equiv \rho r^2/(5 \times 10^{16}\ {\rm g\ cm^{-1}})$, where ρ is the wind density at radius r.

to be the merger of an NS with a white dwarf (McBrien et al. 2019; Gillanders et al. 2020). It was somewhat brighter and longer-lived than the known kilonovae, peaking at $M \approx -18$ mag. However, it still faded much faster than the LFCs (Figure 2) and showed broad metal absorption lines resembling SNe Ic, inconsistent with our events (Figure 4).

Lyutikov & Toonen (2019) proposed that Cow-like RETs can arise from accretion-induced collapse following the merger of a carbon–oxygen white dwarf with an oxygen–neon–magnesium white dwarf. This model produces a magnetar in combination with a low ejecta mass. If one of the white dwarfs retained a surface hydrogen layer (type DA), a residual precollapse wind can help to explain the observed lines in the spectrum of AT 2022aedm. This model may be a plausible progenitor channel for LFCs. However, it also predicts Cow-like nonthermal emission, which is ruled out in the case of AT 2022aedm. This channel also has a short delay time, such that the host galaxies are likely to still be star-forming, in tension with the elliptical hosts of our objects. Brooks et al. (2017) suggested another channel for RETs from the collapse of a long-lived remnant of a helium white dwarf merging with an oxygen–neon white dwarf, though these models were fainter than our LFCs.

Finally, mergers involving a main-sequence or evolved star with a stellar-mass BH have also been suggested as progenitors of Cow-like events. Given the older host environments in LFCs, mergers with Wolf–Rayet stars (Metzger 2022) are probably disfavored in this case. A merger of a BH with a lower-mass He core is more consistent with a long delay time. In this case, the accretion rate is expected to be much lower, though additional luminosity could be produced by interaction of disk winds with stellar material lost earlier in the merger (Metzger & Pejcha 2017).

Kremer et al. (2021, 2023) presented models for tidal disruptions of main-sequence stars by stellar-mass BHs in dense clusters. Some of their wind-reprocessed models exhibit optical rise times and postpeak temperatures similar to LFCs. However, while the bolometric luminosities can reach $\sim 10^{44}$ erg s^{-1}, most of this energy is emitted in the UV and X-ray regime, and none of the models reach the peak optical magnitudes of our objects.

Noting the early similarity of AT 2022aedm to some TDE spectra, we encourage a broader exploration of the parameter space for stellar-mass TDEs. Another important test of TDE models (stellar or intermediate mass) will be identifying globular clusters at the positions of LFCs. The James Webb Space Telescope (JWST) can reach the peak of the globular cluster luminosity function (≈ -7.5 mag; Harris & Racine 1979) in 10 ks with NIRCam for an event within 200 Mpc. At the distance of AT 2022aedm, it is possible to achieve the same constraint in $\approx$100 ks. We note, however, that the angular extent of a typical globular cluster at this distance is comparable to the NIRCam pixel scale, making identification challenging.

5. Conclusions

We have presented a detailed analysis of AT 2022aedm, a very unusual, rapidly evolving transient in a massive elliptical galaxy. It has a rise time of <10 days, a luminous peak of $M_g = -22$ mag, and a fast decline of 2 mag in the subsequent 15 days. The optical colors evolve quickly to the red during the decline phase, while the spectrum remains devoid of identifiable broad features throughout. We do, however, detect narrow emission lines of Hα and He II during the first few days, reminiscent of shock cooling in young SNe, and narrow blueshifted absorption lines at later times.

We identify two previous transients, both with uncertain classifications, that share the key properties of bright peaks, fast declines, strong color evolution, and spectra without high equivalent width emission or absorption lines. This suggests that AT 2022aedm represents a well-observed example of a previously unrecognized class of luminous, fast-cooling events that we term LFCs. All three events occurred in passive galaxies with offsets of $\sim$4–10 kpc.

Their unique combination of properties poses challenges for any physical scenario. The passive environments disfavor a massive star origin, while the light curves and spectra are inconsistent with thermonuclear SNe interacting with a dense medium. Mergers of compact object binaries are unable to reproduce the peak luminosity. Tidal disruption of a star by an intermediate-mass BH, as suggested for Dougie (Vinkó et al. 2015), may struggle to produce the fast color evolution. Instead, we find that these events may be broadly consistent with an extreme shock breakout, though from an as-yet-unknown progenitor. Alternatively, models of TDEs from stellar-mass BHs show promise, though current models emit too much of their luminosity in the UV and X-ray. Refinements of stellar-mass TDE models and searches for dense local environments at the sites of LFCs should help to confirm or rule out this scenario.

Acknowledgments

We thank Brian Metzger, Eliot Quataert, and an anonymous referee for helpful comments that improved this paper. We thank Anna Ho for sharing the data on AT 2020bot. We also thank Joe Bright, Paul Scott, and David Titterington for help with the AMI–LA observations. M.N., A.A., and X.S. are supported by the European Research Council (ERC) under the European Union's Horizon 2020 research and innovation program (grant agreement No. 948381) and by UK Space Agency grant No. ST/Y000692/1. P.R. is supported by STFC grant 2742655. S.J.S. acknowledges funding from STFC grants ST/X006506/1 and ST/T000198/1. T.P. acknowledges the support by ANID through the Beca Doctorado Nacional 202221222222. J.V. is supported by NKFIH-OTKA grant K-142534 from the National Research, Development and Innovation Office, Hungary. T.-W.C. thanks the Max Planck Institute for Astrophysics for hosting her as a guest researcher. M.P. is supported by a research grant (19054) from VILLUM FONDEN. P.C. acknowledges support via an Academy of Finland grant (340613; PI: R. Kotak). P.W. acknowledges support from Science and Technology Facilities Council (STFC) grant ST/R000506/1. M.F. is supported by a Royal Society—Science Foundation Ireland University Research Fellowship. M.K. is partially supported by the program Unidad de Excelencia María de Maeztu CEX2020-001058-M. L.G., C.P.G., M.K., and T.E.M.B. acknowledge support from Unidad de Excelencia María de Maeztu CEX2020-001058-M, Centro Superior de Investigaciones Científicas (CSIC) under PIE project 20215AT016, and the Spanish Ministerio de Ciencia e Innovación (MCIN) and the Agencia Estatal de Investigación (AEI) 10.13039/501100011033 under the PID2020-115253GA-I00 HOSTFLOWS project. L.G. also acknowledges support from the European Social Fund (ESF) "Investing in your future" under the 2019 Ramón y Cajal program RYC2019-027683-I. C.

P.G. also acknowledges financial support from the Secretary of Universities and Research (Government of Catalonia) and by the Horizon 2020 Research and Innovation Programme of the European Union under the Marie Sklodowska-Curie and the Beatriu de Pinós 2021 BP 00168 program. T.E.M.B. also acknowledges financial support from the 2021 Juan de la Cierva program FJC2021-047124-I. G.P.S. acknowledges support from the Royal Society, the Leverhulme Trust, and the Science and Technology Facilities Council (grant Nos. ST/N021702/1 and ST/S006141/1). F.E.B. acknowledges support from ANID-Chile BASAL CATA ACE210002 and FB210003, FONDECYT Regular 1200495, and Millennium Science Initiative Program — ICN12_009.

ATLAS is primarily funded through NASA grants NN12AR55G, 80NSSC18K0284, and 80NSSC18K1575. The ATLAS science products are provided by the University of Hawaii, QUB, STScI, SAAO, and Millennium Institute of Astrophysics in Chile. The Pan-STARRS telescopes are supported by NASA grants NNX12AR65G and NNX14 AM74G. Based on observations collected at the European Organisation for Astronomical Research in the Southern Hemisphere, Chile, as part of ePESSTO+ (the advanced Public ESO Spectroscopic Survey for Transient Objects Survey). The ePESSTO+ observations were obtained under ESO program ID 108.220C (PI: Inserra). This work makes use of data from the Las Cumbres Observatory global network of telescopes. The LCO group is supported by NSF grants AST-1911151 and AST-1911225. The Liverpool Telescope is operated on the island of La Palma by Liverpool John Moores University in the Spanish Observatorio del Roque de los Muchachos of the Instituto de Astrofisica de Canarias with financial support from the UK Science and Technology Facilities Council. We thank the staff of the Mullard Radio Astronomy Observatory for their assistance in the maintenance and operation of AMI, which is supported by the Universities of Cambridge and Oxford. We also acknowledge support from the European Research Council under grant ERC-2012-StG-307215 LODESTONE.

Facilities: NTT, PS1, Liverpool:2m, LCOGT, MMT, Swift, AMI.

Software: Astropy (Astropy Collaboration et al. 2013, 2018), Matplotlib (Hunter 2007), Numpy (Harris et al. 2020), SciPy (Virtanen et al. 2020), Astroquery (Ginsburg et al. 2019), Astrometry.net (Lang et al. 2010), Astroalign (Beroiz et al. 2020), Lacosmic (van Dokkum et al. 2012), Pyzogy (Guevel & Hosseinzadeh 2017), Photutils (Bradley et al. 2020), Superbol (Nicholl 2018), Mosfit (Guillochon et al. 2018), Aladin (Bonnarel et al. 2000), PSF (Nicholl 2023).

ORCID iDs

M. Nicholl https://orcid.org/0000-0002-2555-3192
S. Srivastav https://orcid.org/0000-0003-4524-6883
S. Gomez https://orcid.org/0000-0001-6395-6702
P. Ramsden https://orcid.org/0009-0009-2627-2884
L. Rhodes https://orcid.org/0000-0003-2705-4941
S. J. Smartt https://orcid.org/0000-0002-8229-1731
K. W. Smith https://orcid.org/0000-0001-9535-3199
A. Aamer https://orcid.org/0000-0002-9085-8187
F. E. Bauer https://orcid.org/0000-0002-8686-8737
K. C. Chambers https://orcid.org/0000-0001-6965-7789
P. Charalampopoulos https://orcid.org/0000-0002-0326-6715
T.-W. Chen https://orcid.org/0000-0002-1066-6098
H. Gao https://orcid.org/0000-0003-1015-5367
D. A. Green https://orcid.org/0000-0003-3189-9998
L. Galbany https://orcid.org/0000-0002-1296-6887
M. Gromadzki https://orcid.org/0000-0002-1650-1518
C. P. Gutiérrez https://orcid.org/0000-0003-2375-2064
C. Inserra https://orcid.org/0000-0002-3968-4409
P. G. Jonker https://orcid.org/0000-0001-5679-0695
E. A. Magnier https://orcid.org/0000-0002-7965-2815
C. McCully https://orcid.org/0000-0001-5807-7893
S. L. McGee https://orcid.org/0000-0003-3255-3139
T. Moore https://orcid.org/0000-0001-8385-3727
T. E. Müller-Bravo https://orcid.org/0000-0003-3939-7167
M. Newsome https://orcid.org/0000-0001-9570-0584
E. Padilla Gonzalez https://orcid.org/0000-0003-0209-9246
C. Pellegrino https://orcid.org/0000-0002-7472-1279
T. Pessi https://orcid.org/0000-0001-6540-0767
M. Pursiainen https://orcid.org/0000-0003-4663-4300
A. Rest https://orcid.org/0000-0002-4410-5387
B. J. Shappee https://orcid.org/0000-0003-4631-1149
G. P. Smith https://orcid.org/0000-0003-4494-8277
G. Terreran https://orcid.org/0000-0003-0794-5982
P. Wiseman https://orcid.org/0000-0002-3073-1512
D. R. Young https://orcid.org/0000-0002-1229-2499

References

Abbott, B. P., Abbott, R., Abbott, T. D., et al. 2017, PhRvL, 119, 161101
Albareti, F. D., Allende Prieto, C., Almeida, A., et al. 2017, ApJS, 233, 25
Angus, C. R., Baldassare, V. F., Mockler, B., et al. 2022, NatAs, 6, 1452
Arcavi, I., Gal-Yam, A., Sullivan, M., et al. 2014, ApJ, 793, 38
Arcavi, I., Wolf, W. M., Howell, D. A., et al. 2016, ApJ, 819, 35
Astropy Collaboration, Price-Whelan, A. M., Sipőcz, B. M., et al. 2018, AJ, 156, 123
Astropy Collaboration, Robitaille, T. P., Tollerud, E. J., et al. 2013, A&A, 558, A33
Bellm, E. C., Kulkarni, S. R., Graham, M. J., et al. 2019, PASP, 131, 018002
Beniamini, P., Hotokezaka, K., van der Horst, A., & Kouveliotou, C. 2019, MNRAS, 487, 1426
Berger, E., Fong, W., & Chornock, R. 2013, ApJL, 774, L23
Beroiz, M., Cabral, J. B., & Sanchez, B. 2020, A&C, 32, 100384
Blagorodnova, N., Gezari, S., Hung, T., et al. 2017, ApJ, 844, 46
Bonnarel, F., Fernique, P., Bienaymé, O., et al. 2000, A&AS, 143, 33
Bradley, L., Sipőcz, B., Robitaille, T., et al. 2020, astropy/photutils: v1.0.0, Zenodo, doi:10.5281/zenodo.4044744
Breeveld, A. A., Landsman, W., Holland, S. T., et al. 2011, in AIP Conf. Ser. 1358, Gamma Ray Bursts 2010, ed. J. E. McEnery, J. L. Racusin, & N. Gehrels (Melville, NY: AIP), 373
Bright, J. S., Margutti, R., Matthews, D., et al. 2022, ApJ, 926, 112
Brooks, J., Schwab, J., Bildsten, L., et al. 2017, ApJ, 850, 127
Bruch, R. J., Gal-Yam, A., Schulze, S., et al. 2021, ApJ, 912, 46
Bruch, R. J., Gal-Yam, A., Yaron, O., et al. 2023, ApJ, 952, 119
Burrows, D. N., Hill, J. E., Nousek, J. A., et al. 2005, SSRv, 120, 165
Carnall, A. C., Leja, J., Johnson, B. D., et al. 2019, ApJ, 873, 44
Chambers, K. C., Magnier, E. A., Metcalfe, N., et al. 2016, arXiv:1612.05560
Charalampopoulos, P., Pursiainen, M., Leloudas, G., et al. 2023, A&A, 673, 95
Chen, T.-W., Smartt, S. J., Yates, R. M., et al. 2017, MNRAS, 470, 3566
Chen, Z. H., Yan, L., Kangas, T., et al. 2023, ApJ, 943, 41
Chevalier, R. A., & Irwin, C. M. 2011, ApJL, 729, L6
Coppejans, D. L., Margutti, R., Terreran, G., et al. 2020, ApJL, 895, L23
CASA Team, Bean, B., Bhatnagar, S., et al. 2022, PASP, 134, 114501
De Cia, A., Gal-Yam, A., Rubin, A., et al. 2018, ApJ, 860, 100
Drout, M. R., Chornock, R., Soderberg, A. M., et al. 2014, ApJ, 794, 23
Edge, A., Sutherland, W., Kuijken, K., et al. 2013, Msngr, 154, 32
Evans, P. A., Beardmore, A. P., Page, K. L., et al. 2007, A&A, 469, 379
Evans, P. A., Beardmore, A. P., Page, K. L., et al. 2009, MNRAS, 397, 1177
Fabricant, D., Fata, R., Epps, H., et al. 2019, PASP, 131, 075004
Flewelling, H. A., Magnier, E. A., Chambers, K. C., et al. 2020, ApJS, 251, 7
Fraser, M., Stritzinger, M. D., Brennan, S. J., et al. 2021, arXiv:2108.07278
Frohmaier, C., Angus, C. R., Vincenzi, M., et al. 2021, MNRAS, 500, 5142
Gal-Yam, A. 2019, ARA&A, 57, 305

Gal-Yam, A., Arcavi, I., Ofek, E. O., et al. 2014, Natur, 509, 471
Gal-Yam, A., Bruch, R., Schulze, S., et al. 2022, Natur, 601, 201
Gehrels, N., Chincarini, G., Giommi, P., et al. 2004, ApJ, 611, 1005
Gezari, S., Chornock, R., Rest, A., et al. 2012, Natur, 485, 217
Gillanders, J. H., Sim, S. A., & Smartt, S. J. 2020, MNRAS, 497, 246
Ginsburg, A., Sipőcz, B. M., Brasseur, C. E., et al. 2019, AJ, 157, 98
Ginzburg, S., & Balberg, S. 2012, ApJ, 757, 178
Gkini, A., Pessi, P., Brennan, S., et al. 2022, TNSCR, 2022-3690, 1
Gomez, S., Berger, E., Nicholl, M., Blanchard, P. K., & Hosseinzadeh, G. 2022, ApJ, 941, 107
Gompertz, B. P., Nicholl, M., Smith, J. C., et al. 2023, arXiv:2305.07582
Gottlieb, O., Tchekhovskoy, A., & Margutti, R. 2022, MNRAS, 513, 3810
Guevel, D., & Hosseinzadeh, G. 2017, Dguevel/Pyzogy: Initial Release, v0.0.1, Zenodo, doi:10.5281/zenodo.1043973
Guillochon, J., Manukian, H., & Ramirez-Ruiz, E. 2014, ApJ, 783, 23
Guillochon, J., Nicholl, M., Villar, V. A., et al. 2018, ApJS, 236, 6
Harris, C. R., Millman, K. J., van der Walt, S. J., et al. 2020, Natur, 585, 357
Harris, W. E., & Racine, R. 1979, ARA&A, 17, 241
Hickish, J., Razavi-Ghods, N., Perrott, Y. C., et al. 2018, MNRAS, 475, 5677
Ho, A. Y. Q., Margalit, B., Bremer, M., et al. 2022, ApJ, 932, 116
Ho, A. Y. Q., Perley, D. A., Gal-Yam, A., et al. 2023, ApJ, 949, 120
Ho, A. Y. Q., Perley, D. A., Kulkarni, S. R., et al. 2020, ApJ, 895, 49
Hosseinzadeh, G., Arcavi, I., Valenti, S., et al. 2017, ApJ, 836, 158
Hosseinzadeh, G., Cowperthwaite, P. S., Gomez, S., et al. 2019, ApJL, 880, L4
Hunter, J. D. 2007, CSE, 9, 90
HI4PI Collaboration, Ben Bekhti, N., Flöer, L., et al. 2016, A&A, 594, A116
Irani, I., Prentice, S. J., Schulze, S., et al. 2022, ApJ, 927, 10
Jiang, J.-a., Yasuda, N., Maeda, K., et al. 2022, ApJL, 933, L36
Johnson, B. D., Leja, J., Conroy, C., & Speagle, J. S. 2021, ApJS, 254, 22
Ivezić, Ž., Kahn, S. M., Tyson, J. A., et al. 2019, ApJ, 873, 111
Kasen, D., & Bildsten, L. 2010, ApJ, 717, 245
Khazov, D., Yaron, O., Gal-Yam, A., et al. 2016, ApJ, 818, 3
Kouveliotou, C., Dieters, S., Strohmayer, T., et al. 1998, Natur, 393, 235
Kremer, K., Lu, W., Piro, A. L., et al. 2021, ApJ, 911, 104
Kremer, K., Mockler, B., Piro, A. L., & Lombardi, J. C., Jr 2023, MNRAS, 524, 6358
Lang, D., Hogg, D. W., Mierle, K., Blanton, M., & Roweis, S. 2010, AJ, 139, 1782
Lantz, B., Aldering, G., Antilogus, P., et al. 2004, Proc. SPIE, 5249, 146
Leja, J., Carnall, A. C., Johnson, B. D., Conroy, C., & Speagle, J. S. 2019, ApJ, 876, 3
Leja, J., Johnson, B. D., Conroy, C., van Dokkum, P. G., & Byler, N. 2017, ApJ, 837, 170
Leloudas, G., Patat, F., Maund, J. R., et al. 2015, ApJL, 815, L10
Lunnan, R., Chornock, R., Berger, E., et al. 2014, ApJ, 787, 138
Lunnan, R., Chornock, R., Berger, E., et al. 2018, ApJ, 852, 81
Lyutikov, M., & Toonen, S. 2019, MNRAS, 487, 5618
Maraston, C., Strömbäck, G., Thomas, D., Wake, D. A., & Nichol, R. C. 2009, MNRAS, 394, L107
Margutti, R., & Chornock, R. 2021, ARA&A, 59, 155
Margutti, R., Metzger, B. D., Chornock, R., et al. 2019, ApJ, 872, 18
Margutti, R., Milisavljevic, D., Soderberg, A. M., et al. 2014, ApJ, 797, 107
Matthews, D. J., Margutti, R., Metzger, B. D., et al. 2023, RNAAS, 7, 126
McBrien, O. 2021, PhD thesis, Queen's University Belfast
McBrien, O. R., Smartt, S. J., Chen, T.-W., et al. 2019, ApJL, 885, L23
McMullin, J. P., Waters, B., Schiebel, D., Young, W., & Golap, K. 2007, in ASP Conf. Ser. 376, Astronomical Data Analysis Software and Systems XVI, ed. R. A. Shaw, F. Hill, & D. J. Bell (San Francisco, CA: ASP), 127
Metzger, B. D. 2022, ApJ, 932, 84
Metzger, B. D., & Pejcha, O. 2017, MNRAS, 471, 3200
Mockler, B., Guillochon, J., & Ramirez-Ruiz, E. 2019, ApJ, 872, 151
Nicholl, M. 2018, RNAAS, 2, 230
Nicholl, M. 2023, PSF: photometry-sans-frustration, v1.0, Zenodo, doi:10.5281/zenodo.8205720
Nicholl, M., Guillochon, J., & Berger, E. 2017, ApJ, 850, 55
Nicholl, M., Smartt, S. J., Jerkstrand, A., et al. 2015, MNRAS, 452, 3869
Nicholl, M., Wevers, T., Oates, S. R., et al. 2020, MNRAS, 499, 482
Nugent, P. E., Sullivan, M., Cenko, S. B., et al. 2011, Natur, 480, 344
Ofek, E. O., Rabinak, I., Neill, J. D., et al. 2010, ApJ, 724, 1396
Pastorello, A., Smartt, S. J., Mattila, S., et al. 2007, Natur, 447, 829
Perley, D. A., Ho, A. Y. Q., Yao, Y., et al. 2021, MNRAS, 508, 5138
Perley, D. A., Mazzali, P. A., Yan, L., et al. 2019, MNRAS, 484, 1031
Perley, D. A., Quimby, R. M., Yan, L., et al. 2016, ApJ, 830, 13
Perley, D. A., Sollerman, J., Schulze, S., et al. 2022, ApJ, 927, 180
Poznanski, D., Prochaska, J. X., & Bloom, J. S. 2012, MNRAS, 426, 1465
Prentice, S. J., Ashall, C., James, P. A., et al. 2019, MNRAS, 485, 1559
Prentice, S. J., Maguire, K., Smartt, S. J., et al. 2018, ApJL, 865, L3
Pritchard, T. A., Bensch, K., Modjaz, M., et al. 2021, ApJ, 915, 121
Pursiainen, M., Childress, M., Smith, M., et al. 2018, MNRAS, 481, 894
Quimby, R. M., Kulkarni, S. R., Kasliwal, M. M., et al. 2011, Natur, 474, 487
Rastinejad, J. C., Gompertz, B. P., Levan, A. J., et al. 2022, Natur, 612, 223
Rest, A., Garnavich, P. M., Khatami, D., et al. 2018, NatAs, 2, 307
Roming, P. W. A., Kennedy, T. E., Mason, K. O., et al. 2005, SSRv, 120, 95
Schlafly, E. F., & Finkbeiner, D. P. 2011, ApJ, 737, 103
Schulze, S., Krühler, T., Leloudas, G., et al. 2018, MNRAS, 473, 1258
Shappee, B. J., Prieto, J. L., Grupe, D., et al. 2014, ApJ, 788, 48
Shingles, L., Smith, K. W., Young, D. R., et al. 2021, TNSAN, 7, 1
Silverman, J. M., Nugent, P. E., Gal-Yam, A., et al. 2013, ApJS, 207, 3
Skrutskie, M. F., Cutri, R. M., Stiening, R., et al. 2006, AJ, 131, 1163
Smartt, S. J., Valenti, S., Fraser, M., et al. 2015, A&A, 579, A40
Smith, K. W., Smartt, S. J., Young, D. R., et al. 2020, PASP, 132, 085002
Smith, N., & McCray, R. 2007, ApJL, 671, L17
Srivastav, S., Smartt, S. J., Huber, M. E., et al. 2022, MNRAS, 511, 2708
Tampo, Y., Tanaka, M., Maeda, K., et al. 2020, ApJ, 894, 27
Tanvir, N. R., Levan, A. J., Fruchter, A. S., et al. 2013, Natur, 500, 547
Tonry, J., Denneau, L., Weiland, H., et al. 2022, TNSTR, 2022-3680, 1
Tonry, J. L., Denneau, L., Heinze, A. N., et al. 2018, PASP, 130, 064505
Tucker, M. A., Shappee, B. J., Huber, M. E., et al. 2022, PASP, 134, 124502
van Dokkum, P. G., Bloom, J., & Tewes, M. 2012, L.A.Cosmic: Laplacian Cosmic Ray Identification, Astrophysics Source Code Library, ascl:1207.005
Vinkó, J., Yuan, F., Quimby, R. M., et al. 2015, ApJ, 798, 12
Virtanen, P., Gommers, R., Oliphant, T. E., et al. 2020, NatMe, 17, 261
Whitesides, L., Lunnan, R., Kasliwal, M. M., et al. 2017, ApJ, 851, 107
Wiseman, P., Pursiainen, M., Childress, M., et al. 2020, MNRAS, 498, 2575
Wright, E. L., Eisenhardt, P. R. M., Mainzer, A. K., et al. 2010, AJ, 140, 1868
Yao, Y., Ho, A. Y. Q., Medvedev, P., et al. 2022, ApJ, 934, 104
Yaron, O., & Gal-Yam, A. 2012, PASP, 124, 668
Zackay, B., Ofek, E. O., & Gal-Yam, A. 2016, ApJ, 830, 27
Zwart, J. T. L., Barker, R. W., Biddulph, P., et al. 2008, MNRAS, 391, 1545